A Robust Numerical Solution of the Stochastic Collection–Breakup Equation for Warm Rain

OLIVIER P. PRAT AND ANA P. BARROS

Pratt School of Engineering, Civil and Environmental Engineering Department, Duke University, Durham, North Carolina

(Manuscript received 18 September 2006, in final form 3 January 2007)

ABSTRACT

The focus of this paper is on the numerical solution of the stochastic collection equation–stochastic breakup equation (SCE–SBE) describing the evolution of raindrop spectra in warm rain. The drop size distribution (DSD) is discretized using the fixed-pivot scheme proposed by Kumar and Ramkrishna, and new discrete equations for solving collision breakup are presented. The model is evaluated using established coalescence and breakup parameterizations (kernels) available in the literature, and in that regard this paper provides a substantial review of the relevant science. The challenges posed by the need to achieve stable and accurate numerical solutions of the SCE–SBE are examined in detail. In particular, this paper focuses on the impact of varying the shape of the initial DSD on the equilibrium solution of the SCE–SBE for a wide range of rain rates and breakup kernels. The results show that, although there is no dependence of the equilibrium DSD on initial conditions for the same rain rate and breakup kernel, there is large variation in the time that it takes to reach steady state. This result suggests that, in coupled simulations of in-cloud motions and microphysics and for short time scales (<30 min) for which transient conditions prevail, the equilibrium DSD may not be attainable except for very heavy rainfall. Furthermore, simulations for the same initial conditions show a strong dependence of the dynamic evolution of the DSD on the breakup parameterization. The implication of this result is that, before the debate on the uniqueness of the shape of the equilibrium DSD can be settled, there is critical need for fundamental research including laboratory experiments to improve understanding of collisional mechanisms in DSD evolution.

1. Introduction

Many attempts have been made over the years to describe the evolution of rainfall microstructure in the presence of coalescence, breakup, accretion, evaporation, and condensation mechanisms. Mainly two types of numerical methods are used for the prediction of the drop size distribution (DSD) evolution in atmospheric modeling—discrete methods and moments approaches. In the discrete approach, the continuous DSD is approximated by a finite number of size classes. In the moments' approach, the droplet spectrum is represented by selected statistical moments of the DSD.

The method of moments was introduced by Enukashvili (1964) to solve the stochastic collection equation (SCE) using a set of differential equations written in terms of the moments of the DSD and a linear approximation for the probability distribution function. Because of the fact that the linear approximation resulted in negative values over some discrete intervals, Tzivion et al. (1987) proposed that the closure of the equations be achieved by relationships linking higher-order moments with the two lowest-order moments.

Bleck (1970) describes an efficient discrete approach to solve the SCE by using a geometric grid for the discretization. This method was later applied to simulate collision-induced breakup [stochastic breakup equation (SBE)] by List and Gillespie (1976). Brown (1993) used a similar sectional approach for solving the combined SCE–SBE and included drop evaporation processes. As compared with a regular grid, Bleck's geometric grid permits the use of fewer scalar variables (one scalar for each size section), and thus the computational requirements are reduced. Early numerical models describing the evolution of the DSD followed Bleck's method (List and Gillespie 1976). However, the accuracy of the solution is strongly dependent on the degree of resolution of the discretization grid (Bleck

Corresponding author address: Dr. Ana P. Barros, Duke University, Box 90287, 2457 CIEMAS Fitzpatrick Bldg., Durham, NC 27708.
E-mail: barros@duke.edu

DOI: 10.1175/JAM2544.1

1970; Hu and Srivastava 1995, hereinafter HS95). HS95 modified Bleck's method by using a centered mass average density, defined as the average of "forward" (Bleck's method) and "backward" mass-weighted drop concentrations, in order to counter the numerical diffusivity of Bleck's method. Another caveat of Bleck's technique is that the scheme is internally consistent with regard to mass but does not conserve other moments of the DSD. Other modelers adopted the technique of Gelbard and Seinfeld (1978), which was modified to include collisional breakup (List et al. 1987; List and McFarquhar 1990; McFarquhar 2004, hereinafter MF04). Gelbard and Seinfeld (1978) proposed a finite-element method combined with orthogonal collocation to solve the population balance equation. The main drawbacks of the collocation method are a relatively high computational cost and the nonpreservation of the integral properties of the DSD (Mahoney and Ramkrishna 2002). Alternatively, the approach proposed by Kovetz and Olund (1969) preserves both number and mass of the DSD but suffers from the same numerical diffusivity as that of other approaches (e.g., Bleck's method, Gelbard and Seinfeld's method).

Diffusivity in the form of artificial broadening of the DSD spectra remains the Achilles' heel of discrete solutions of the SCE–SBE. Berry and Reinhardt (1974) proposed a numerical scheme for the resolution of the SCE that overcomes this challenge by estimating the distribution function at intermediate points of the discretization grid using a six-point Lagrangian interpolation. The scheme proposed by Berry and Reinhardt (1974) is accurate for the SCE (Khain et al. 2000); however, it incurs high computational costs relative to other discrete approaches and the method of moments. Moreover, it does not respect mass conservation, and thus its integration into general cloud models with detailed microphysics may cause large uncertainties (Bott 1998).

The goal of this study is to develop an efficient and robust discrete method that will be internally consistent with regard to selected moments of the DSD. In particular, the use of a numerical scheme capable of accurately tracking the total liquid water content of drops is essential in the perspective of future implementation into cloud models. The discretization method adopted here is based on the fixed-pivot technique proposed by Kumar and Ramkrishna (1996, hereinafter KR96) for population balance models in chemical engineering. This approach preserves the internal consistency of the solution with regard to two moments of a population of particles (raindrops in our case). The method is flexible enough to allow the selection of any two moments of the DSD that should be preserved (drop number density concentration, total water content, radar reflectivity, etc.) as well as the topology of the discretization grid (geometric, regular, partially or fully irregular). This last property is especially useful to describe the tail region of the DSD (i.e., at the higher end of drop diameters where the raindrop number density presents a steep variation). Local refinements of the grid are possible with the same level of computational effort.

The paper is organized as follows. First, a description of the model and the numerical methods used to solve the SCE–SBE is provided. Next, we review several breakup parameterizations (kernels) used in this work. Last, results obtained with the model will be compared and discussed with prior work in the peer-reviewed literature. Analytical and algebraic equations required for the model are presented with the objective of providing the next generation of modelers with a starting point for subsequent work.

2. Model description for the resolution of the SCE–SBE

a. General formulation of the SCE–SBE

The general governing equation for the evolution of the DSD in the presence of coalescence and collisional breakup can be expressed as (HS95)

$$\frac{\partial n(v)}{\partial t} = \frac{1}{2}\int_0^v n(v-v',t)n(v',t)C(v-v',v')\,dv' - n(v,t)\int_0^\infty n(v',t)C(v,v')\,dv' + \frac{1}{2}\int_0^\infty n(v',t)\,dv'\int_0^\infty n(v'',t)B(v',v'')P(v,v',v'')\,dv'' - n(v,t)\int_0^\infty \frac{n(v'',t)B(v',v'')}{v+v''}\,dv''\int_0^{v+v''} v'P(v',v,v'')\,dv' = I_1 - I_2 + I_3 - I_4, \quad (1)$$

where I_1 and I_2 are, respectively, the source and sink terms associated with coalescence and I_3 and I_4 are, respectively, the source and sink terms associated with breakup. In more detail, I_1 accounts for the generation

of droplets of volume v resulting from coalescence of smaller droplets, and I_2 describes the removal of droplets of volume v resulting from coalescence with other droplets. Additionally, I_3 describes the generation of droplets of volume v resulting from collisional breakup of other droplets, and I_4 accounts for the removal of droplets of volume v resulting from collisional breakup. The coalescence kernel $C(v, v')$ in I_1 and I_2 is defined by

$$C(v, v') = K(v, v')E_{\text{coal}}(v, v') \quad \text{and} \tag{2}$$

$$K(v, v') = (9\pi/16)^{1/3}(v^{1/3} + v'^{1/3})^2|\mathbf{V} - \mathbf{V}'|E_{\text{coal}}(v, v'), \tag{3}$$

where $K(v, v')$ is the gravitational collision kernel (Pruppacher and Klett 1978), and $E_{\text{coal}}(v, v')$ is the coalescence efficiency for two colliding drops of volume v and v' (Low and List 1982a).

The gravitational collision kernel $K(v, v')$ describes the rate at which the space occupied by a droplet of volume v' (and fall velocity $\mathbf{V}'$) is intercepted and swept out by a droplet of volume v (and fall velocity $\mathbf{V}$). The fall velocity of individual raindrops is estimated here following Best (1950):

$$\mathbf{V} = 943\{1 - [\exp(-d/17.7)]^{1.147}\}, \tag{4}$$

where $\mathbf{V}$ is in centimeters per second and d, the diameter of the drop, is in centimeters; $E_{\text{coal}}(v, v')$ is the collision efficiency. For the drop sizes considered in this study ($d \geq 0.01$ cm), $E_{\text{coal}}(v, v') = 1$, as per Long (1974).

The breakup kernel $B(v, v')$ in terms I_3 and I_4 is expressed as follows:

$$B(v, v') = K(v, v')E_{\text{brkp}}(v, v') = K(v, v')[1 - E_{\text{coal}}(v, v')], \tag{5}$$

where E_{brkp} is the breakup efficiency. In Eq. (1), $P(v, v', v'')$ describes the fragment distribution function, and the product $P(v, v', v'')dv$ quantifies the number of drops in the volume interval between v and $v + dv$ resulting from the collisional breakup of two drops of volume v' and v''. Elementary mass conservation requirements dictate that

$$\begin{aligned} P(v, v', v'') &= 0 \quad \text{if} \quad v > v' + v'' \\ &\geq 0 \quad \text{if} \quad 0 < v < v' + v'' \end{aligned} \tag{6}$$

and

$$\int_0^{v'+v''} vP(v, v', v'')\, dv = v' + v''. \tag{7}$$

When the conditions in Eqs. (6) and (7) are fulfilled by the breakup function $P(v, v', v'')$, the loss term resulting from collisional breakup I_4 can be rewritten in the simplest form,

$$I_4 = n(v, t)\int_0^{\infty} n(v', t)B(v, v')\, dv'. \tag{8}$$

b. Discrete formulation of the general SCE–SBE

The continuous general SCE–SBE [Eq. (1)] is discretized using the fixed-pivot technique proposed by KR96. KR96 applied their method to spontaneous breakup only; here, the framework is extended for the first time to collisional breakup. Full derivation of the discrete equations to preserve any two selected moments of the DSD is presented in appendix A.

To determine which two moments of the DSD should be selected for solving the SCE–SBE using the fixed-pivot technique, two combinations of moments of order 0 (number), 1 (mass), and 2 (proportional to the radar reflectivity factor) were investigated thorough numerical experimentation (not shown): (0, 1); (1, 2). From the first principles, mass should always be conserved. The selection of the other moment depends on the governing dynamics of coalescence and breakup processes. When coalescence is dominant, there is an advantage to conserving the second-order moment in order to better capture the evolution of the tail of the DSD at larger drop sizes, that is, combination (1, 2). On the contrary, in case of pure or dominant breakup, the conservation of drop number is more appropriate. Overall, the number/mass conservative scheme (0, 1) was found to be more suitable for the case of combined coalescence–breakup mechanisms, and for all coalescence/breakup kernels tested.

The integration of Eq. (1) over the ith discrete interval defined between volumes v_i and v_{i+1} yields

$$\begin{aligned} \frac{dN_i(t)}{dt} = &\sum_{\substack{j,k \\ x_{i-1} \leq v = (x_j + x_k) \leq x_{i+1}}}^{j \geq k} (1 - 1/2\delta_{j,k})\eta C_{j,k}N_j(t)N_k(t) - N_i(t)\sum_{k=1}^{\text{NBIN}} C_{i,k}N_k(t) + \frac{1}{2}\sum_{j=1}^{\text{NBIN}} N_j(t)\sum_{k=1}^{\text{NBIN}} N_k(t)B_{i,k}\kappa_{i,j,k} \\ &- N_i(t)\sum_{k=1}^{\text{NBIN}} B_{i,k}N_k(t), \end{aligned} \tag{9}$$

with

$$N_i(t) = \int_{v_i}^{v_{i+1}} n(v, t)\, dv, \tag{10}$$

$$C_{j,k} = C(x_j, x_k), \quad \text{and} \tag{11}$$

$$B_{i,k} = B(x_i, x_k), \tag{12}$$

where $\delta_{j,k}$ is the Dirac function.

The term η in Eq. (9) is the contribution to the ith interval of the DSD from the coalescence of two droplets of volume x_j and x_k. To preserve the zeroth and first-order moments of the DSD (respectively, number and mass), η is calculated as follows:

$$\eta = \frac{x_{i+1} - v}{x_{i+1} - x_i} \quad \text{if} \quad x_i \le v \le x_{i+1} \quad \text{and} \quad \eta = \frac{v - x_{i-1}}{x_i - x_{i-1}} \quad \text{if} \quad x_{i-1} \le v \le x_i. \tag{13}$$

In this implementation, the fixed-pivot technique (KR96) applied to the coalescence part (SCE) of the general SCE–SBE is comparable to the discrete method of Kovetz and Olund (1969) in that a drop of volume v generated by coalescence is distributed proportionally to both adjacent discrete drop diameter classes conserving both number and mass. The fixed-pivot technique (KR96) can be seen therefore as a generalization of Kovetz and Olund (1969) that allows the extension of the discretization technique to the conservation of two (or potentially more) selected integral properties (moments) of the DSD.

The term $\kappa_{i,j,k}$ in Eq. (9) is the contribution to droplet population located at the ith interval resulting from the collisional breakup of two drops of volume x_j and x_k. For number and mass preservation, $\kappa_{i,j,k}$ is given by

$$\kappa_{i,j,k} = \int_{x_i}^{x_{i+1}} \frac{x_{i+1} - v}{x_{i+1} - x_i} P(v, x_j, x_k)\, dv + \int_{x_{i-1}}^{x_i} \frac{v - x_{i-1}}{x_i - x_{i-1}} P(v, x_j, x_k)\, dv. \tag{14}$$

For cases in which the two integrals in Eq. (14) cannot be evaluated analytically, a simple numerical integration is performed. The average number density of droplets ($\text{cm}^{-3}\ \text{cm}^{-1}$) for the ith interval is given by

$$\overline{n}_i(t) = \frac{1}{d_{i+1} - d_i} \int_{v_i}^{v_{i+1}} n(v, t)\, dv = \frac{N_i(t)}{d_{i+1} - d_i}, \tag{15}$$

where $N_i(t)$ is in cubic centimeters and diameters d_i and d_{i+1} are in centimeters. Last, the kth-order moment of the DSD is given by the following formula:

$$M_k = \sum_{i=1}^{\text{NBIN}} N_i(t) m_i^k, \tag{16}$$

where m_i is the drop mass in grams of the ith class category. From Eq. (16), we obtain the drop number concentration ($M_{k=0}$; cm^{-3}), the total water volume content ($M_{k=1}$; g cm^{-3}), and the radar reflectivity factor $\{Z = [6/(\rho\pi)]^2 10^{12}$, proportional to $M_{k=2}$ in millimeters to the sixth power per meter cubed$\}$.

3. Breakup parameterizations

In this section, we describe the breakup kernels used in this work. Collisional breakup is treated using the Low and List (1982a,b, hereinafter LL82a,b) parameterization as well as the new parameterization recently proposed by MF04. The exponential breakup kernel (Feingold et al. 1988, hereinafter FTL88) and the aerodynamical breakup (Srivastava 1971, hereinafter SR71) are also analyzed.

a. Aerodynamical breakup contribution in the SCE–SBE

SR71 provides an expression for the breakup of large drops where the probability of breakup of a drop of volume v and diameter d (cm) is given by

$$P(v) = 2.94E - 0.7 \exp(17d). \tag{17}$$

The distribution function resulting from a breakup event is given by

$$Q(v', v) = \frac{ab}{3v} \left(\frac{d}{d'}\right) \exp\left(-b \frac{d}{d'}\right), \tag{18}$$

with a and b being constants. The quantity $Q(v', v)dv$ corresponds to the number of drops with a mass between v and $(v + dv)$ (diameter d) that are created by the spontaneous disintegration of a drop of volume v' (diameter d'). The constants ($a = 62.3$, $b = 7$) have been determined from fitting experimental data (Komabayasi et al. 1964) and adjusted to enforce mass conservation. The discrete expression for aerodynamical breakup contribution (SBE) is derived in appendix A.

b. Collisional breakup contribution in the SCE–SBE

1) Exponential fragment distribution function (FTL88)

FTL88 proposed an exponential breakup function $P(v, v', v'')$ that has the property of respecting mass conservation requirements [Eqs. (6) and (7)],

$$P(v, v', v'') = (nM_0/M_1)^2(v' + v'') \exp(-nM_0/M_1 v), \tag{19}$$

where n is a constant, M_0 (cm^{-3}) is the initial number of drops, and M_1 (g cm^{-3}) is the initial water content. Despite the lack of experimental basis, this fragment distribution function provides a physical representation of the collisional breakup mechanism consistent with observations. In addition to the respect of mass conservation for each pair of colliding drops (v', v''), the number of drops created $P(v, v', v'')$ increases with decreasing diameter d. For a given diameter d, the number of drops created by collisional breakup increases with the initial mass ($v' + v''$) involved in the collisional breakup event.

2) The Low and List parameterization (LL82a,b)

McTaggart-Cowan and List (1975) performed collision experiments that were later completed by Low and List (1982a). Two drops of different size were forced to collide, and the resulting fragment distribution function was recorded using a high-speed camera. McTaggart-Cowan and List (1975) observed three major types of breakup that they reported as filament, disc, and sheet breakup types. A parameterization of the fragment distribution function $P(v, v', v'')$ was proposed based on these experimental data (LL82a,b; correction by List et al. 1987). For each type of breakup, the fragment distribution function was expressed as the sum of one (sheet and disc breakup) or two (filament breakup) Gaussian functions to describe the remaining parent drop(s), and a lognormal function to describe the distribution of the satellite droplets created by the breakup. The overall fragment distribution function $P(d, \text{dl}, \text{ds})$ is obtained from the weighted contributions of each breakup type involving two drops of diameter (large: dl) and (small: ds), and is given by

$$P(d, \text{dl}, \text{ds}) = R_{\text{FI}}P_{\text{FI}}(d, \text{dl}, \text{ds}) + R_{\text{DI}}P_{\text{DI}}(d, \text{dl}, \text{ds}) + R_{\text{SH}}P_{\text{SH}}(d, \text{dl}, \text{ds}), \tag{20}$$

where R_{FI}, R_{DI}, and R_{SH} are, respectively, the proportion of breakup events that occur as filament, disc, and sheet, such that

$$R_{\text{FI}} + R_{\text{DI}} + R_{\text{SH}} = 1. \tag{21}$$

The Gaussian and lognormal functions for each breakup type (X = FI, DI, and SH) are as follows:

$$P_{X,\text{GAU}}(d, \text{dl}, \text{ds}) = H_{\text{GAU}}(\text{dl}, \text{ds}) \exp\left\{-\left[\frac{d - \mu_{\text{GAU}}(\text{dl}, \text{ds})}{\sqrt{2}\sigma_{\text{GAU}}(\text{dl}, \text{ds})}\right]^2\right\} \tag{22}$$

and

$$P_{X,\text{LGN}}(d, \text{dl}, \text{ds}) = \frac{H_{\text{LGN}}(\text{dl}, \text{ds})}{d} \exp\left\{-\left[\frac{\ln d - \mu_{\text{LGN}}(\text{dl}, \text{ds})}{\sqrt{2}\sigma_{\text{LGN}}(\text{dl}, \text{ds})}\right]^2\right\}. \tag{23}$$

The determination of the overall fragment distribution function [Eq. (20)] requires the separate determination for each component of three parameters (H, μ, σ), where H is the height of the distribution, μ is the modal diameter, and σ is the width of the distribution. Overall, a total of 21 parameters must be determined to describe the general fragment distribution function. As pointed out by previous studies (Valdez and Young 1985, hereinafter VY85; Brown 1997), one of the limitations of the LL82a,b parameterization is that it does not fully respect mass conservation for single-breakup events involving two drops. For each colliding drop pair (dl, ds), the zero-level requirement is that the sum of the mass of the two colliding drops needs to be equal to the sum of all drops created after the collisional event [Eq. (7)]. VY85 and Brown (1997) proposed adjustments of the LL82a,b parameterization to enforce the mass conservation constraint. To simplify the determination of the parameters H, μ, and σ the narrow Gaussian functions (i.e., Gaussian functions describing the remaining parent drops for filament and sheet breakup) were replaced by a modified delta function centered on the original parent size, reducing to 15 the total number of parameters (VY85):

$$P_{X,\text{DLT}}(d, \text{dl}, \text{ds}) = H_{\text{DLT}}(\text{dl}, \text{ds})\delta(d - \mu). \tag{24}$$

For the determination of the 15 parameters mentioned above, we follow closely VY85 as follows:

1) For each colliding drop pair dl and ds the ratio for each type of breakup R_{FI}, R_{DI}, and R_{SH} is calculated based on the LL82a,b parameterization. Some scaling adjustments are necessary for drop pairs for which the parameterization returns a ratio greater than 100% for the sum of all breakup types as per List et al. (1987), in contradiction to Eq. (21).
2) The number of drops created from a colliding pair of drops dl and ds is computed for each breakup type F_{FI}, F_{SH}, and F_{DI} from the LL82a,b parameterization (LL82a,b; List et al. 1987). When the value obtained is smaller than 2 (i.e., less than two drops potentially created for a colliding pair dl and ds), no breakup is considered and collisions are treated as bouncing interactions. In this case, the final fragment distribution function is the same as the initial one, and corresponds to the sum of two delta functions [Eq. (24)] centered around parent drop sizes (dl) and (ds) with height equal to unity.
3) The coefficients H_{LGN}, μ_{LGN}, and σ_{LGN} of the satellite fragment distribution functions are calculated iteratively based on the total number of drops. A simple Newton method is used for the determination (LL82a,b; List et al. 1987) of the width σ_{LGN} of the lognormal function [Eq. (23)], whereas other parameters, μ_{LGN} and H_{LGN} are updated at each intermediate iteration. If the solution does not converge, the collision dl and ds is treated as a bouncing interaction.

When a solution is attained and parameters H_{LGN}, μ_{LGN}, and σ_{LGN} are determined, mass conservation is checked for every drop pair and every breakup type. Scaling adjustments are applied to verify the limit conditions to the satellite distribution proposed by VY85 in the case of filament and sheet breakups. The mass of the remaining parent drop(s) is adjusted by the height of the distribution H in such a way that the mass is conserved for every breakup event.

Last, the general fragment distribution function [Eq. (20)] is computed and integrated over every bin category to obtain the term $\kappa_{i,j,k}$ [Eq. (14)] in the positive breakup term of the discrete SCE–SBE [$I_{3i}(t)$ in Eq. (9)]. An analytical integration is performed for the breakup function over each size class (bin). See appendix B for the details on the calculation of the definite integral over a bin size for generalized Gaussian and lognormal distributions.

3) THE MCFARQUHAR PARAMETERIZATION (MF04)

Previously, the strategy followed to enforce mass conservation for the collisional breakup mechanism in LL82a,b as well as the numerical approach (discrete method vs method of moments) was found to have a significant influence on the final steady-state DSD (VY85; List et al. 1987; FTL88; HS95; Brown 1997; MF04). In addition, the extension of the LL82a,b parameterization for some arbitrary pair of drops dl and ds cannot be justified from physical principles. MF04 proposed a new parameterization derived from the original experimental data of LL82a,b by adopting the same combination of lognormal, Gaussian, and modified delta functions for the expression of the fragment size distribution [Eq. (20)]. The novel aspect of this new parameterization is the use of a modified Monte Carlo technique with bootstrap to randomly choose the results of individual collisions of arbitrary pairs of drops. New expressions for mode μ, standard deviation σ, and height H of these distributions were derived from such simulations (MF04). Among the advantages of the MF04 parameterization is the fact that it has a more consistent physical basis than the LL82a,b parameterization to generalize experimental results of collisional breakup. In addition, by providing analytical expressions for the parameters H, σ, and μ of the fragment distribution function, MF04 overcomes the challenge posed by the LL82a,b parameterization to enforce mass conservation for each single-breakup event (VY85; Brown 1997; HS95).

4. Analysis of modeling results

Modeling results analyzed next were obtained by using a single box model to track the evolution of the DSD over time assuming spatial homogeneity of the DSD (List and McFarquhar 1990; HS95). The temporal evolution of the DSD is tracked by performing a numerical integration using a simple forward Eulerian scheme ($\Delta t = 2$ s). Additional details concerning the numerical stability of the algorithm will be reported in the next section.

a. Aerodynamical breakup

Figure 1 displays the solution of the SCE–SBE for the aerodynamical breakup kernel (SR71). The results are presented for a geometric grid with a ratio ($s = 1.25$). The initial DSD is a Marshall–Palmer (MP; Marshall and Palmer 1948) distribution given by

$$n_D(d, t = 0) = N_0 \exp(-\Lambda d), \tag{25}$$

with

$$\Lambda = 41R^{-0.21}, \tag{26}$$

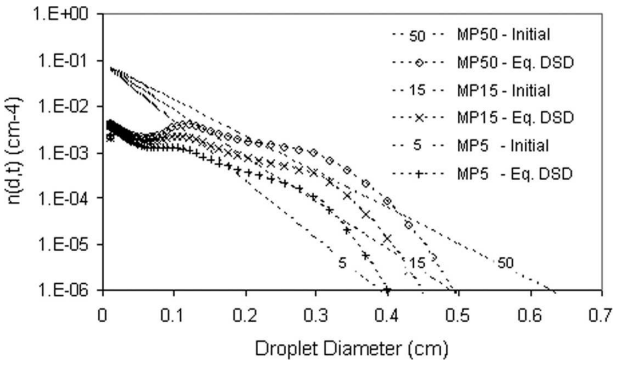

FIG. 1. Equilibrium DSD for the solution of the SCE–SBE for an aerodynamical breakup kernel (SR71). The solution is obtained for a geometric grid ($s = 1.25$). Results are presented for three initial Marshall–Palmer DSDs with rain rates of $R = 5$, 15, and 50 mm h^{-1}.

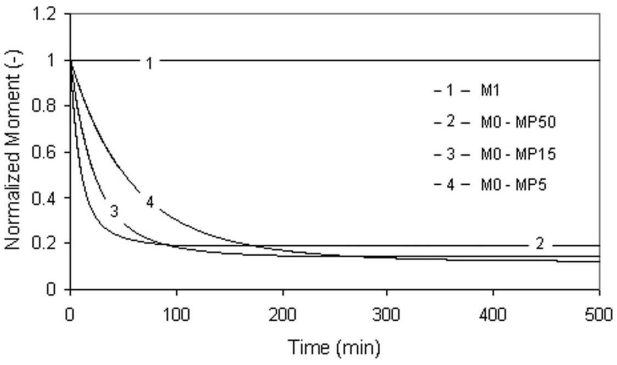

FIG. 2. Evolution of the normalized moments (M_0 and M_1) of the DSD. Results are presented for three initial Marshall–Palmer DSD with rain rates of $R = 5$, 15, and 50 mm h^{-1}. The normalized moment M_1 (mass conservation indicator) remains constant throughout the simulation.

where $n_D(d, t = 0)$ is the raindrop distribution (by unit of diameter) expressed in cubic centimeters per centimeter. The raindrop diameter d is in centimeters, R is the rain rate (mm h^{-1}), and N_0 is a constant ($N_0 = 0.08$ cm^{-4}). The results are presented for three values of the rain rate ($R = 5$, 15, and 50 mm h^{-1}) corresponding to episodes of light, intermediate, and heavy rainfall, respectively, for initial water contents of 3.4×10^{-7}, 8.7×10^{-7}, and 2.4×10^{-6} g cm^{-3}. Results show that steady state is achieved in approximately 400, 180, and 100 min, respectively, for light, intermediate, and heavy rain rates. The determination of the time necessary to reach equilibrium is based on the evolution of the first moment (M_0). Figure 2 displays the evolution of the moments M_0 and M_1 of the DSD. Note that M_1 (mass conservation indicator) indeed remains unchanged throughout the simulation. With the combined effects of coalescence and breakup, the normalized values for M_0 at equilibrium are comparable and equal to 1.23 (i.e., 3.2×10^{-5} g cm^{-3}), 1.28 (i.e., 6.0×10^{-5} g cm^{-3}), and 1.88 (i.e., 1.3×10^{-4} g cm^{-3}) for $R = 5$, 15, and 50 mm h^{-1}, respectively.

b. *Collisional breakup using an exponential fragment distribution function*

The numerical results obtained for the SCE–SBE [Eqs. (9)–(16)] with the FTL88 breakup function are presented in Fig. 3 for an initial Marshall–Palmer distribution and three values of the rain rate ($R = 5$, 15, and 50 mm h^{-1}). The equilibrium DSDs exhibit only one peak located at 0.061, 0.078, and 0.1 cm for $R = 5$, 15, and 50 mm h^{-1}, respectively. The slope of the equilibrium DSD at larger drop sizes ranges from 125 cm^{-1} ($R = 50$ mm h^{-1}) to 140 cm^{-1} ($R = 5$ mm h^{-1}). The time necessary to reach equilibrium increases with decreasing rain rate R, respectively, 65, 30, and 17 min for $R = 5$, 15, and 50 mm h^{-1}. The characteristics of the equilibrium DSD obtained with the FTL88 kernel are reported in Table 1, and Table 2 summarizes the properties of the equilibrium DSD, such as the droplet number density M_0 and the radar reflectivity factor Z. Note that, for the FTL88 kernel, the DSD evolves from an initial MP distribution to a distribution exponential in mass with the same liquid water content as initially.

c. *Collisional breakup using the Low and List parameterization*

Figure 4 displays the evolution of the DSD in the presence of coalescence and breakup for an initial DSD using a Marshall–Palmer distribution and a rain rate of $R = 50$ mm h^{-1} following LL82a,b. Steady state is achieved in 25 min. The equilibrium DSD presents two

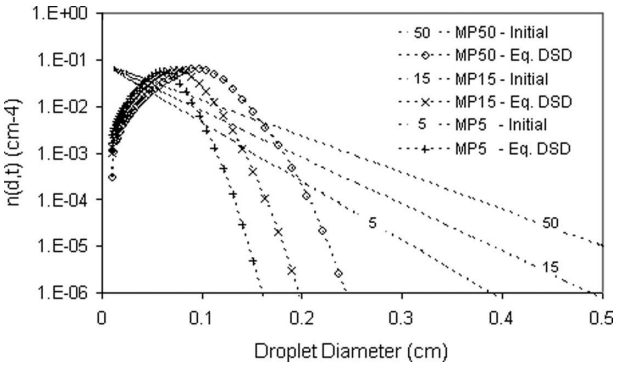

FIG. 3. Equilibrium DSD for the solution of the SCE–SBE for an exponential breakup kernel (FTL88; $n = 2$). Results are presented for three initial Marshall–Palmer DSDs with rain rates $R = 5$, 15, and 50 mm h^{-1}. The solution is obtained with a geometric grid ($s = 1.25$).

TABLE 1. Summary of the characteristics of the equilibrium DSD derived from box models. The results were obtained using a geometric grid with a parameter $s = 1.25$.

Case	Initial distribution			Peaks		Slope (cm^{-1})	Breakup function
	Type	R (mm h^{-1})	M_1 (g m^{-3})	No.	d (cm)		
1 of this paper	MP	5	0.34	1	0.061	140	FTL88
2 of this paper	MP	15	0.87	1	0.078	130	FTL88
3 of this paper	MP	50	2.40	1	0.1	125	FTL88
4 of this paper	MP	5	0.34	2	0.026–0.08	72	LL82a,b
5 of this paper	MP	15	0.87	2	0.026–0.08	72	LL82a,b
6 of this paper	MP	50	2.40	2	0.026–0.08	68	LL82a,b
7 of this paper	MP	5	0.34	2	0.026–0.25	65	MF04
8 of this paper	MP	15	0.87	2	0.026–0.25	65	MF04
9 of this paper	MP	50	2.40	2	0.026–0.25	62	MF04
MF04	MP	54	≈2.4	2	0.026–0.23		MF04
List and McFarquhar (1990)	MP	54	≈2.4	3	0.026–0.091–0.18		LL82a,b
VY85	MP	35	1.80	3	0.03–0.08–0.20	66	LL82a,b

distinct peaks located at 0.26 and 0.8 mm. Other authors have reported similar equilibrium DSDs presenting two or three peaks (List et al. 1987; FTL88; HS95; Brown 1997). A survey of the shape of the steady-state DSD of previous studies can be found in HS95. Concerning the equilibrium DSD, it is worth mentioning that researchers using a Joss–Waldvogel disdrometer (JWD; e.g., de Beauville et al. 1988; Zawadzky and de Agostinho Antonio 1988) have recorded equilibrium DSD presenting peaks located at drop diameters similar to those predicted by numerical models using the LL82a,b parameterization (VY85; List et al. 1987; FTL88; List and McFarquhar 1990; HS95; Brown 1997). However, Sheppard (1990) showed that DSD measurements performed with a JWD presented artifacts caused by imperfect calibration and the misplacement of the bin diameter limits. After a recalibration, the recorded peaks disappeared, consistent with McFarquhar and List (1993), who showed that the recorded DSD was essentially identical to an MP distribution when nonlinearity effects of the JWD signal processing unit were corrected. The debate concerning the existence or nonexistence of multiple peaks in the equilibrium DSD is still open. No observations under natural conditions have confirmed or denied the existence or absence of secondary peaks for the equilibrium DSD itself (Testik and Barros 2007). In numerical models, the equilibrium DSD as well as the location and existence of two or three peaks depends on the method used to enforce mass conservation and the underlying kernels. Here, we follow the method proposed by VY85. The equilibrium DSD obtained by VY85 showed three peaks located at 0.03, 0.08, and 0.20 cm. However, in this study, we do not find the presence of a peak located in the large drop size range. Closer inspection of the slope of the DSD does not show any change in curvature at a droplet diameter located around $d = 0.20$ cm. However, for $d \geq 0.18/0.19$ cm, the equilibrium DSD

TABLE 2. Summary of integral properties of the equilibrium DSD derived from box models. The results were obtained using a geometric grid with a parameter $s = 1.25$.

Case	Initial distribution (MP)			Equilibrium distribution		t_{eq} (min)	Breakup function
	Type	R (mm h^{-1})	M_1 (g m^{-3})	M_0 (m^{-3})	Z (mm^6 m^{-1})		
1 of this paper	MP	5	0.34	2.5×10^3	3.2×10^2	≈40	FTL88
2 of this paper	MP	15	0.87	3.3×10^3	1.5×10^3	≈15	FTL88
3 of this paper	MP	50	2.40	4.4×10^3	8.5×10^3	≈5	FTL88
4 of this paper	MP	5	0.34	1.0×10^3	6.4×10^3	≈200	LL82a,b
5 of this paper	MP	15	0.87	2.6×10^3	1.6×10^4	≈120	LL82a,b
6 of this paper	MP	50	2.40	5.4×10^3	4.4×10^4	≈30	LL82a,b
7 of this paper	MP	5	0.34	1.2×10^3	9.5×10^3	≈350	MF04
8 of this paper	MP	15	0.87	2.9×10^3	2.4×10^4	≈150	MF04
9 of this paper	MP	50	2.40	7.9×10^3	6.2×10^4	≈40	MF04
MF04	MP	54	≈2.4	8.6×10^3	4.7×10^4		MF04
List and McFarquhar (1990)	MP	54	≈2.4	4.1×10^3	3.5×10^4	40	LL82a,b

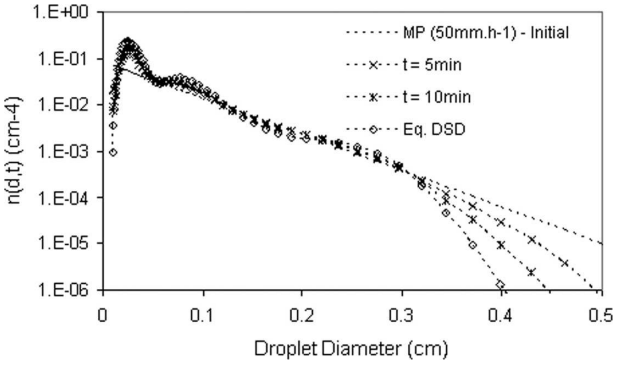

FIG. 4. DSD evolution for the solution of the SCE–SBE for the LL82a,b fragment distribution function. The solution is obtained with a geometric grid ($s = 1.25$). The initial Marshall–Palmer DSD has a rain rate of $R = 50$ mm h^{-1}.

presents a shoulder before an exponential decrease for larger drop sizes ($d \geq 0.3$ cm).

Figure 5 displays the equilibrium DSD for an initial Marshall–Palmer distribution and three values of the rain rate ($R = 5$, 15, and 50 mm h^{-1}). Regardless of the initial rain rate, the equilibrium DSD exhibits the same features with two peaks located at 0.026 and 0.08 cm and the same shoulder for $d \geq 0.18/0.19$ cm. In addition, the slopes of the DSD for larger drops are comparable and range from 68 ($R = 50$ mm h^{-1}) to 72 cm^{-1} ($R = 5$ mm h^{-1}). Table 1 summarizes the simulated characteristics of the equilibrium DSD obtained for different values of the rain rate R.

Furthermore, the equilibrium achieved is independent from the initial DSD. That is, for the same initial water content, a similar equilibrium DSD was obtained for different initial DSDs (Marshall–Palmer, exponential with regard to the drop mass distribution). For long enough simulation times, all spectra collapse to the same equilibrium DSD, as expected. The significant difference concerns the time that is necessary to reach this equilibrium DSD (Table 2). Because of the short-time time scales characteristic of transient conditions in real clouds, this result raises the question of whether the equilibrium DSD is attainable, but for the most intense rainfall rates (>50 mm h^{-1}).

As mentioned earlier, one of the features of the discretization scheme used in the model is that it allows the selection of different grid topologies (geometric, regular, irregular). A grid sensitivity study is summarized in Fig. 6. Figure 6 displays results for three values of the geometric grid parameter ($s = 1.25$, 1.5, 2) with respectively 60, 32, and 18 bins covering a diameter range from 0.01 to approximately 0.75 cm. The inset shows the equilibrium DSD in the small drop diameter range for regular grids with diameter intervals ($\Delta d =$ 0.01, 0.02, 0.04 cm) and 75, 36, and 19 bins (respectively). In the case of geometric grids, even for a coarse resolution ($s = 2$), the locations of the peaks are well captured independently of the value of the grid parameter *s:* the peak locations remain unchanged at 0.026 and 0.08 cm, with the same shoulder for $d \geq 0.18/0.19$ cm. By contrast, in the case of a regular grid (inset Fig. 6), the smallest peak is not captured with the coarsest grid ($\Delta d = 0.04$ cm) and is shifted toward larger drop diameters for the intermediate grid ($\Delta d = 0.02$ cm). Nevertheless, as it concerns the domain of the largest drops (tail of the spectra), regular grids (not shown in Fig. 6) exhibit smaller numerical diffusivity than geometric grids. Indeed, it is a well established fact that the fixed-pivot technique (KR96) and similar discrete approaches (Kovetz and Olund 1969; Bleck 1970) are nu-

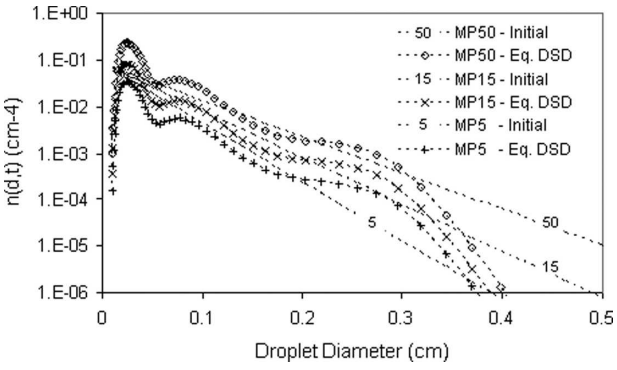

FIG. 5. Equilibrium DSD for the solution of the SCE–SBE for the LL82a,b fragment distribution function. Results are presented for three initial Marshall–Palmer DSDs with rain rates $R = 5$, 15, and 50 mm h^{-1}. The solution is obtained with a geometric grid ($s = 1.25$).

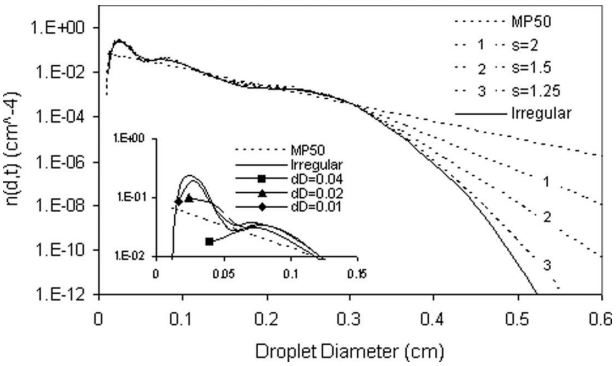

FIG. 6. Equilibrium DSD of the SCE–SBE for the LL82a,b fragment distribution function. Results are presented for different grids type and resolutions: geometric ($s = 1.25$, 1.5, 2), regular in diameter ($\Delta d = 0.01$, 0.02, 0.04 cm), and irregular [i.e., combination of a geometric grid ($s = 2$) at small drop diameter and a regular grid ($\Delta d = 0.02$ cm) at large drop diameter]. The initial Marshall–Palmer DSD has a rain rate of $R = 50$ mm h^{-1}.

merically diffusive. The artificial broadening of the DSD is particularly important for pure (or dominant) coalescence regimes (SCE) where the front of the DSD evolves constantly toward larger drop sizes. To counter numerical diffusivity in the discrete approach, Bott (1998) proposed a flux correction method that was tested by Khain et al. (2000) for solving the SCE. However, for combined coalescence breakup (SCE–SBE), the adaptation of Bott's method would be both computationally prohibitive and a challenge to implement because of the difficult estimation of the breakup function under this discretization scheme (Seifert et al. 2005). In addition, in the case of combined coalescence–breakup (SCE–SBE), the numerical diffusivity problem caused by the evolution of the DSD toward larger sizes driven by coalescence is alleviated by simultaneous breakup that erodes the front tail of the distribution. Alternatively, numerical diffusivity effects are reduced and an improved description of the DSD can be achieved by increasing the number of bin categories, or by grid refinements for a low computational cost (e.g., the number of elementary computations inside a time loop being proportional to the third power of the number of bins). Typically, a geometric grid with $s = 1.25$ ($s \approx 2^{1/3}$) can describe accurately the DSD as reported in previous studies (HS95). An example of grid adaptability is presented in Fig. 6 for the equilibrium DSD obtained with an irregular grid (40 bins) that combines a geometric grid ($s = 2$) at small drop sizes ($d \leq 0.1$ cm) to capture the local peaks, and a regular grid ($\Delta d = 0.02$ cm) at larger drop sizes ($d \geq 0.1$ cm) to capture accurately the tail of the DSD. Relative to a fine geometric grid ($s = 1.25$), the description of the tail is significantly improved (slope of 70 cm^{-1} for $s = 2.0$ vs 68 cm^{-1} for $s = 1.25$) with a smaller number of bins (40 vs 60).

Another aspect of the numerical efficiency of the algorithm presented in this work is its remarkable numerical stability. A time step sensitivity analysis has been performed with time steps of $\Delta t = 1$, 5, 10, 30, and up to 60 s, and no change was observed either in the shape of the equilibrium DSD, or in the time necessary to reach steady state in the evolution of the moments of the distribution. Implementation of discrete methods for the prediction of combined coalescence–breakup (Bleck's method, Gelbard and Seinfeld's method) must use very small time steps ($\Delta t = 1$ s) to maintain numerical stability (List et al. 1987; List and McFarquhar 1990; HS95; MF04). The method proposed by Berry and Reinhardt (1974) appears to be sensitive to numerical instabilities even for very small time steps of $\Delta t = 1$ s (Bott 1998), whereas the method of moments accommodates larger time steps (e.g., $\Delta t = 3$ s in FTL88). The numerical cost increases for the latter because it requires solving a set of differential equations for the moments of the distribution instead of a single equation for the evolution of the drop number density. The robust numerical stability of the model presented here is an advantage for future implementation in a general cloud dynamics model.

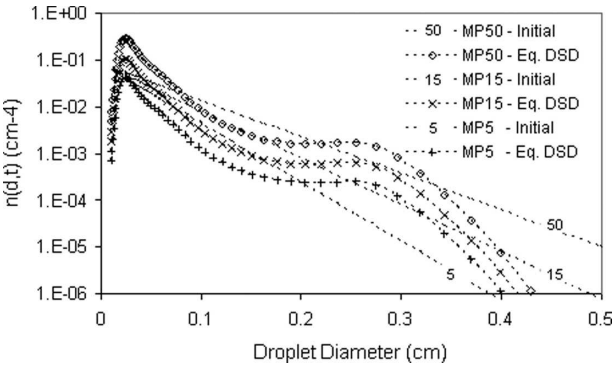

FIG. 7. Equilibrium DSD for the solution of the SCE–SBE for the MF04 breakup function. Results are presented for three initial Marshall–Palmer DSDs with rain rates $R = 5$, 15, and 50 mm h^{-1}. The solution is obtained with a geometric grid ($s = 1.25$).

d. The McFarquhar parameterization

Results using the new parameterization proposed by MF04 are shown in Fig. 7 for an initial Marshall–Palmer distribution and three values of the rain rate ($R = 5$, 15, and 50 mm h^{-1}). Regardless of the value of the rain rate, the most important difference is that the equilibrium DSD is different from the steady state obtained with LL82a,b, although it still shows a two-peak-only curve, with peaks located at 0.026 and 0.25 cm. This is consistent with the results of MF04 who reported a bimodal distribution with peaks located at 0.026 and 0.23 cm. In addition, the MF04 equilibrium DSD presents a higher proportion of drops of small sizes in comparison with the equilibrium DSD obtained with LL82a,b. Considering the first peak location at 0.026 cm, the height of the peak of the DSD obtained with MF04 is 30% higher than the peak obtained with LL82a,b in our case, as compared with that approximately 130% higher obtained by MF04 for similar rain rates ($R = 50$ mm h^{-1}, $R = 54$ mm h^{-1}). The presence of a larger proportion of small drops in MF04 relative to LL82a,b breakup kernels might lead to an increased role of coalescence in the DSD evolution, although we find a lesser effect than that of MF04. In addition, when the evaporation process is taken into consideration, the smoothing effect of the equilibrium DSD observed by Brown (1993) with the LL82a,b parameterization might have a longer

time scale for the MF04 breakup kernel, thus allowing better detection of the eventual presence of a peak located in the small-diameter range.

As for the results obtained with the LL82a,b breakup function (Fig. 5), the equilibrium DSD using MF04 exhibits the same trend regardless of the value of the rain rate, and the same bimodal equilibrium DSD is achieved with peaks located at 0.026 and 0.025 cm. The slope of the DSD found at larger drop sizes ranges from 62 ($R = 50$ mm h^{-1}) to 65 cm^{-1} ($R = 5$ mm h^{-1}), which is slightly lower than the results obtained with LL82a,b. Characteristics of the equilibrium DSD obtained with the MF04 kernel are reported in Table 1.

Table 2 summarizes the values of the integral properties of the equilibrium DSD obtained with the two breakup functions (LL82a,b; MF04) for three values of the rain rate R. Regardless of the value of the rain rate, the droplet concentration is higher with the MF04 method than with the LL82a,b parameterization, as in MF04. However, the difference is smaller in our simulation. Indeed, the difference in drop concentration M_0 was found to be about 10%–50% between the two methods, as compared with 100% at a rain rate of $R = 54$ mm h^{-1} in MF04. Regardless of the value of the rain rate R, the value of the radar reflectivity factor Z is found to be higher with the MF04 kernel than with the LL82a,b parameterization. A difference of about 30% is found between the two methods for the value of Z. The values obtained for Z at $R = 50$ mm h^{-1} are on the same order of magnitude as those obtained by MF04 at $R = 54$ mm h^{-1}. A difference of about 20%–25% is found for the value of Z [$Z = 4.4 \times 10^4$ mm^6 m^{-1} (LL82a,b) and $Z = 6.2 \times 10^4$ mm^6 m^{-1} (MF04), this study] to be compared with $Z = 3.5 \times 10^4$ mm^6 m^{-1} (LL82a,b) and $Z = 4.7 \times 10^4$ mm^6 m^{-1} (MF04), respectively. In addition, the time necessary to achieve steady state increases with decreasing rain rate R. HS95 noted a similar behavior and found equilibrium times ranging from 40 to 4 min for rain rates varying from 17 to 275 mm h^{-1}, respectively. In this study, the time necessary for attaining equilibrium ranges from approximately 200 ($R = 5$ mm h^{-1}) to 25 min ($R = 50$ mm h^{-1}). Regardless of the value of the rain rate R, the time scale of equilibrium is significantly higher using the MF04 kernel relative to the LL82a,b breakup function as reported in Table 2. Under real rain conditions, the observation of multimodal distributions might not be always possible. Favorable conditions for the eventual presence of peaks in the observed DSD would require a sufficient number of collision–breakup events (e.g., important fall distance and high rain rates) in order to allow the development of observable peaks. The important values of the time scales reported in Table 2 in case of light and intermediate rain rates would lead to observed DSDs close to equilibrium DSDs only for exceptional atmospheric conditions. In addition, if the peak located in the small-diameter range ($d = 0.026$ cm) is distinguishable after a relatively short simulation time (between 1 and 2 min for heavy rain rates), and even for intermediate to light rain rates (between 2 and 5 min), the presence of this peak might not be identified because of either detection limits of the instruments for the lower part of the DSD, or evaporation.

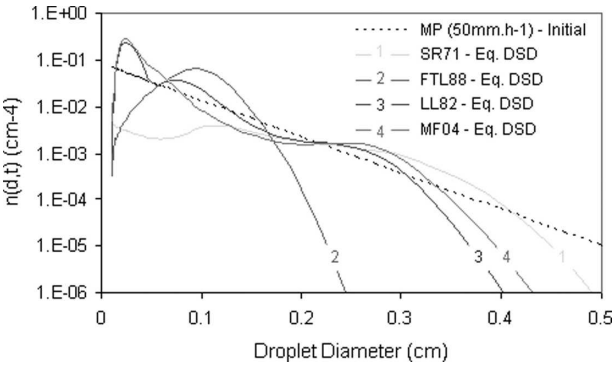

FIG. 8. Equilibrium DSD for the solution of the SCE–SBE for various breakup kernels (SR71; FTL88; LL82a,b; MF04). The solution is obtained with a geometric grid ($s = 1.25$). The initial Marshall–Palmer DSD has a rain rate $R = 50$ mm h^{-1}.

e. Dependence on the breakup kernels

Figure 8 displays the equilibrium DSDs for all breakup kernels considered in the present work (SR71; FTL88; LL82a,b; MF04) and for an initial Marshall–Palmer DSD with a rain rate $R = 50$ mm h^{-1}. The results show that the equilibrium DSD is strongly dependent on the breakup function used in the numerical simulation. In the case of aerodynamical breakup only (SR71), larger drops remain in the equilibrium DSD, whereas for collisional breakup they vanish. The difference is even more dramatic when comparing with the exponential breakup function (FTL88). Also note that, independently of the discretization grid selected, the tail of the steady-state DSD obtained with the modified parameterization proposed by MF04 is always heavier for larger drops than the equilibrium DSD obtained with the original LL82a,b parameterization. Last, regardless of the value of the rain rate R, steeper DSDs are found with LL82a,b than with MF04, even if those values are comparable with a difference of about 5–7 cm^{-1} between the two methods (Table 1).

Independent of the collisional breakup kernel considered (FTL88; LL82a,b; MF04), the time required to reach the equilibrium DSD increases with decreasing

rain rate R or initial water content. For higher values of the volume water content, the coalescence–breakup mechanism is enhanced by the higher initial concentration of water drops, consistent with previous studies (List and McFarquhar 1990; HS95). As mentioned previously, for any initial water content, the shape of the initial DSD (Marshall–Palmer, exponential in mass, etc.) also has an impact on the time necessary to reach equilibrium, but not on the steady-state DSD.

5. Summary and conclusions

A discrete model for the resolution of the stochastic equation for the evolution of the DSD in warm rain is discussed. The model is stable enough to handle large time steps and mass is conserved rigorously—two necessary conditions for a successful implementation in general cloud dynamics models with detailed microphysics. The numerical model was tested using many of the coalescence and breakup kernels available in the literature, including aerodynamical and collisional breakup (LL82a,b). Results are presented for a range of rain rates from light to heavy rainfall, and the parameterization proposed by MF04 was used for comparison. The equilibrium DSD obtained with MF04 leads to a higher droplet number concentration with the creation of more drops of small sizes, a higher radar reflectivity factor, and a heavier right-hand-side tail (large drops) in comparison with the equilibrium DSD obtained with the LL82a,b parameterization.

For both MF04 and LL82a,b parameterizations, a bimodal equilibrium DSD was obtained with a first peak located at a drop diameter of 0.026 cm. However, the location of the second peak differs dramatically between the two methods at 0.08 cm for LL82a,b and 0.25 cm for MF04. Everything else being equal, the location of the second DSD mode (larger or smaller diameter), or even the possible establishment of a clearly identifiable third peak, is dependent on rain rate. Model simulations suggest that the third mode forms for light, long-duration rainfall events, which may happen only in particular environments, such as in the case of stratiform orographic precipitation in the presence of strong synoptic forcing (see, e.g., Lang and Barros 2002). Although the same equilibrium DSD was attained for model simulations forced by different initial DSDs when rain rate and the breakup kernel were the same, there was large variation in the time required to reach steady state. This result suggests that in coupled simulations of in cloud motions and microphysics, and for short time scales (<30 min) when transient conditions prevail, the equilibrium DSD may not be attainable. Last, the sensitivity experiments show strong dependence of the DSD dependence on the breakup kernels used in the SCE–SBE. This reflects the limitations that result from relying on one limited dataset (LL82a,b) for generalizing breakup dynamics. Future progress toward a more accurate description of the evolution of the DSD requires updated coalescence and breakup kernels, and therefore a more comprehensive database of experimental observations are necessary to achieve further progress.

The numerical model presented in this work is currently being extended to include mechanisms such as accretion, evaporation, condensation, and ice formation. In addition, the single box model presented in this paper is already implemented as a column model to be used in the interpretation of laboratory experiments and vertically pointing radars (Prat and Barros 2007).

Acknowledgments. This research was supported in part by Grants NSF ATM 97-530093 and NASA NNG04GP02G with the second author, and by the Pratt School of Engineering.

APPENDIX A

Derivation of Discrete Equations in Order to Conserve Two Integral Properties Using the Fixed-Pivot Technique (KR96)

The intermediate steps for the derivation of discrete equations to conserve two selected integral properties of the DSD are reviewed here. The discretization method uses the fixed-pivot technique proposed by KR96 for combined coalescence–spontaneous breakup. Here, new expressions for the extension of the fixed-pivot technique to collisional breakup are presented.

a. Conservation of two properties of the DSD

When a drop of volume v ($x_i < v < x_{i+1}$) is formed by either coalescence or breakup, the newly created drop will not always have a volume v matching a characteristic size of the discretization grid. The conservation of integral properties of the DSD requires the new drop to be assigned to both adjacent classes (i.e., x_i and x_{i+1}), such that moments of interest are conserved. Fractional number of drops $a(v, x_i)$ and $b(v, x_{i+1})$ are assigned to adjacent class size categories x_i and x_{i+1}, respectively, and must satisfy the following equations for the following moments of kth [Eq. (A1)] and lth [Eq. (A2)] order:

$$a(v, x_i)x_i^k + b(v, x_{i+1})x_{i+1}^k = v^k \quad \text{and} \qquad \text{(A1)}$$

$$a(v, x_i)x_i^l + b(v, x_{i+1})x_{i+1}^l = v^l. \qquad \text{(A2)}$$

By substitution, we obtain for $a(v, x_i)$ and $b(v, x_{i+1})$

$$a(v, x_i) = \frac{v^k x_{i+1}^l - v^l x_{i+1}^k}{x_i^k x_{i+1}^l - x_i^l x_{i+1}^k} \quad \text{and}$$

$$b(v, x_{i+1}) = \frac{v^l x_i^k - v^k x_i^l}{x_{i+1}^l x_i^k - x_{i+1}^k x_i^l}. \tag{A3}$$

b. Terms for collisional breakup

1) BIRTH TERM (I_3)

The source term resulting from collisional breakup,

$$I_3 = \frac{1}{2}\int_{v_i}^{v_{i+1}} dv \int_0^\infty n(v', t)\, dv' \int_0^\infty P(v, v', v'')n(v'', t)B(v', v'')\, dv'', \tag{A4}$$

is modified to

$$I_3 = \frac{1}{2}\int_{x_i}^{x_{i+1}} a(v, x_i)\, dv \int_0^\infty n(v', t)\, dv' \int_0^\infty P(v, v', v'')n(v'', t)B(v', v'')\, dv''$$
$$+ \frac{1}{2}\int_{x_{i-1}}^{x_i} b(v, x_i)\, dv \int_0^\infty n(v', t)\, dv' \int_0^\infty P(v, v', v'')n(v'', t)B(v', v'')\, dv''. \tag{A5}$$

The number density $n(v, t)$ is expressed by

$$n(v, t) = \sum_{k=1}^{\text{NBIN}} N_k(t)\delta(v - x_k). \tag{A6}$$

If we substitute $n(v', t)$ and $n(v'', t)$ by Eq. (A6) in Eq. (A5), we obtain

$$I_3 = \frac{1}{2}\int_{x_i}^{x_{i+1}} a(v, x_i)\, dv \int_0^\infty \left[\sum_{j=1}^{\text{NBIN}} N_j(t)\delta(v' - x_j)\right] dv' \int_0^\infty P(v, v', v'')\left[\sum_{k=1}^{\text{NBIN}} N_k(t)\delta(v'' - x_k)\right] B(v', v'')\, dv''$$
$$+ \frac{1}{2}\int_{x_{i-1}}^{x_i} b(v, x_i)\, dv \int_0^\infty \left[\sum_{j=1}^{\text{NBIN}} N_j(t)\delta(v' - x_j)\right] dv' \int_0^\infty P(v, v', v'')\left[\sum_{k=1}^{\text{NBIN}} N_k(t)\delta(v'' - x_k)\right] B(v', v'')\, dv''. \tag{A7}$$

Giving

$$I_3 = \frac{1}{2}\sum_{j=1}^{\text{NBIN}} N_j(t) \sum_{k=1}^{\text{NBIN}} N_k(t) \int_{x_i}^{x_{i+1}} a(v, x_i)P(v, x_j, x_k)B(x_j, x_k)\, dv$$
$$+ \frac{1}{2}\sum_{j=1}^{\text{NBIN}} N_j(t) \sum_{k=1}^{\text{NBIN}} N_k(t) \int_{x_{i-1}}^{x_i} b(v, x_i)P(v, x_j, x_k)B(x_j, x_k)\, dv, \tag{A8}$$

with $B(x_j, x_k) = B_{j,k}$, we obtain

$$I_3 = \frac{1}{2}\sum_{j=1}^{\text{NBIN}} N_j \sum_{k=1}^{\text{NBIN}} N_k B_{j,k}\left[\int_{x_i}^{x_{i+1}} a(v, x_i)P(v, x_j, x_k)\, dv + \int_{x_{i-1}}^{x_i} b(v, x_i)P(v, x_j, x_k)\, dv\right]. \tag{A9}$$

The substitution of terms $a(v, x_i)$ and $b(v, x_i)$ gives

$$I_3 = \frac{1}{2}\sum_{j=1}^{\text{NBIN}} N_j \sum_{k=1}^{\text{NBIN}} N_k B_{j,k}\kappa_{i,j,k}. \tag{A10}$$

The term $\kappa_{i,j,k}$ is the contribution to population located at the ith representative size from the collisional breakup involving two drops of volume x_j and x_k:

$$\kappa_{i,j,k} = \int_{x_i}^{x_{i+1}} \frac{v^k x_{i+1}^l - v^l x_{i+1}^k}{x_i^k x_{i+1}^l - x_i^l x_{i+1}^k} P(v, x_j, x_k)\, dv + \int_{x_{i-1}}^{x_i} \frac{v^l x_{i-1}^k - v^k x_{i-1}^l}{x_i^l x_{i-1}^k - x_i^k x_{i-1}^l} P(v, x_j, x_k)\, dv. \tag{A11a}$$

For number ($k = 0$) and mass conservation ($l = 1$), we obtain

$$\kappa_{i,j,k} = \int_{x_i}^{x_{i+1}} \frac{x_{i+1} - v}{x_{i+1} - x_i} P(v, x_j, x_k)\, dv + \int_{x_{i-1}}^{x_i} \frac{v - x_{i-1}}{x_i - x_{i-1}} P(v, x_j, x_k)\, dv. \tag{A11b}$$

The above equation is valid for $2 \le i \le \text{NBIN} - 1$. For $i = 1$, $\kappa_{i,j,k}$ is reduced to the first term; for $i = \text{NBIN}$, $\kappa_{i,j,k}$ is reduced to the second term. In this work, the fragment distribution function $P(v, x_j, x_k)$ is a combina-

tion of delta, lognormal, and Gaussian functions, and the evaluation of integral terms in Eqs. (A11a) or (A11b) is performed analytically by the mean of general expressions provided in appendix B.

2) REMOVAL TERM (I_4)

For a fragment distribution function $P(v, v', v'')$, the removal (sink) term resulting from collisional breakup

$$I_4 = \int_{v_i}^{v_{i+1}} n(v,t)\,dv \int_0^{\infty} n(v',t)B(v,v')\,dv' \quad \text{(A12)}$$

is modified to

$$I_4 = \int_{x_i}^{x_{i+1}} a(v,x_i)n(v,t)\,dv \int_0^{\infty} n(v',t)B(v,v')\,dv' + \int_{x_{i-1}}^{x_i} b(v,x_i)\,dv n(v,t) \int_0^{\infty} n(v',t)B(v,v')\,dv'. \quad \text{(A13)}$$

Replacing the number density $n(v,t)$ and $n(v',t)$ by Eq. (A6) and substituting $a(x_i, x_i)$ and $b(x_i, x_i)$ by Eq. (A3), we obtain

$$I_4 = N_i(t) \sum_{k=1}^{\text{NBIN}} B_{i,k} N_k(t). \quad \text{(A14)}$$

c. Coalescence terms

1) SOURCE TERM (TERM I_1)

The birth term resulting from collisional breakup

$$I_1 = \frac{1}{2} \int_{v_i}^{v_{i+1}} dv \int_0^{\infty} n(v-v',t)n(v',t)C(v-v',v')\,dv' \quad \text{(A15)}$$

is modified to

$$I_1 = \frac{1}{2} \int_{x_i}^{x_{i+1}} a(v,x_i)\,dv \int_0^{\infty} n(v-v',t)n(v',t)C(v-v',v')\,dv' + \frac{1}{2} \int_{x_{i-1}}^{x_i} b(v,x_i)\,dv \int_0^{\infty} n(v-v',t)n(v',t)C(v-v',v')\,dv'. \quad \text{(A16)}$$

With the expression of the number density $n(v - v', t)$ and $n(v', t)$ given by Eq. (A6), Eq. (A16) is transformed into

$$I_1 = \frac{1}{2} \int_{x_i}^{x_{i+1}} a(v,x_i)\,dv \int_0^{\infty} \left\{ \sum_{j=1}^{\text{NBIN}} N_j(t)\delta[(v-v') - x_j] \right\} \left[\sum_{k=1}^{\text{NBIN}} N_k(t)\delta(v' - x_k) \right] C(v-v',v')\,dv' + \frac{1}{2} \int_{x_{i-1}}^{x_i} b(v,x_i)\,dv \int_0^{\infty} \left\{ \sum_{j=1}^{\text{NBIN}} N_j(t)\delta[(v-v') - x_j] \right\} \left[\sum_{k=1}^{\text{NBIN}} N_k(t)\delta(v' - x_k) \right] C(v-v',v')\,dv'. \quad \text{(A17)}$$

With $C(x_j, x_k) = C_{j,k}$, we obtain

$$I_1 = \sum_{\substack{j,k \\ x_{i-1} \le v = x_j + x_k \le x_{i+1}}}^{j \ge k} (1 - 1/2\delta_{j,k})\eta C_{j,k} N_j(t) N_k(t). \quad \text{(A18)}$$

The term η is the contribution to the droplet population located at the ith interval resulting from the creation of a drop of volume $(v = x_j + x_k)$ after coalescence of two drops of volume x_j and x_k, respectively,

$$\eta = \frac{v^k x_{i+1}^l - v^l x_{i+1}^k}{x_i^k x_{i+1}^l - x_i^l x_{i+1}^k} \quad \text{if} \quad x_i \le v \le x_{i+1} \quad \text{and} \quad \eta = \frac{v^l x_{i-1}^k - v^k x_{i-1}^l}{x_i^l x_{i-1}^k - x_i^k x_{i-1}^l} \quad \text{if} \quad x_{i-1} \le v \le x_i. \quad \text{(A19a)}$$

For number $(k = 0)$ and mass conservation $(l = 1)$, η is given by

$$\eta = \frac{x_{i+1} - v}{x_{i+1} - x_i} \quad \text{if} \quad x_i \le v \le x_{i+1} \quad \text{and} \quad \eta = \frac{v - x_{i-1}}{x_i - x_{i-1}} \quad \text{if} \quad x_{i-1} \le v \le x_i. \quad \text{(A19b)}$$

2) REMOVAL TERM (I_2)

The discrete formulation of the removal (sink) term resulting from drop coalescence is similar to the death term resulting from breakup (I_4), when replacing $B(v, v')$ by $C(v, v')$:

$$I_2 = N_i(t) \sum_{k=1}^{\text{NBIN}} C_{i,k} N_k(t). \tag{A20}$$

d. Terms of the SCE–SBE for aerodynamical breakup

In the case of aerodynamical breakup, the coalescence contribution remains unchanged (terms I_1 and I_2) while the breakup contribution [i.e., terms I_3 and I_4 in Eq. (1)] is replaced by

$$\frac{\partial n(v)}{\partial t} = \int_v^\infty n(v', t) P(v') Q(v', v)\, dv' - n(v, t) P(v), \tag{A21}$$

where $P(v)$ is the probability of breakup of a drop of volume v, and $Q(v', v)$ is the distribution function resulting from the breakup of a drop of volume v. Mass conservation considerations require that

$$\int_0^v v' Q(v', v)\, dv' = v. \tag{A22}$$

1) REMOVAL TERM (I_4)

The removal (sink) term resulting from aerodynamical breakup

$$I_4 = \int_{v_i}^{v_{i+1}} P(v) n(v, t)\, dv \tag{A23}$$

is simply modified into

$$I_4 = N_i(t) P_i, \tag{A24}$$

with

$$P_i = P(x_i). \tag{A25}$$

2) BIRTH TERM (I_3)

The birth term resulting from aerodynamical breakup

$$I_3 = \int_{v_i}^{v_{i+1}} \int_v^\infty n(v', t) P(v') Q(v', v)\, dv' \tag{A26}$$

is modified to

$$I_3 = \int_{x_i}^{x_{i+1}} a(v, x_i)\, dv \int_v^\infty n(v', t) P(v') Q(v', v)\, dv' + \int_{x_{i-1}}^{x_i} b(v, x_i)\, dv \int_v^\infty n(v', t) P(v') Q(v', v)\, dv'. \tag{A27}$$

Replacing the number density $n(v', t)$ by Eq. (A6) and substituting $a(x_i, x_i)$ and $b(x_i, x_i)$ by Eq. (A3), Eq. (A27) is transformed into

$$I_3 = \sum_{k=i}^{\text{NBIN}} N_k(t) P_k n_{i,k}. \tag{A28}$$

The term $n_{i,k}$ is the contribution to droplet population located at the ith interval resulting from the breakup of a droplet of volume x_k,

$$n_{i,k} = \int_{x_i}^{x_{i+1}} \frac{v^k x_{i+1}^l - v^l x_{i+1}^k}{x_i^k x_{i+1}^l - x_i^l x_{i+1}^k} Q(x_k, v)\, dv + \int_{x_{i-1}}^{x_i} \frac{v^l x_{i-1}^k - v^k x_{i-1}^l}{x_i^l x_{i-1}^k - x_i^k x_{i-1}^l} Q(x_k, v)\, dv. \tag{A29a}$$

For conservation of drop number ($k = 0$) and mass ($l = 1$), the term $n_{i,k}$ is given by

$$n_{i,k} = \int_{x_i}^{x_{i+1}} \frac{x_{i+1} - v}{x_{i+1} - x_i} Q(x_k, v)\, dv + \int_{x_{i-1}}^{x_i} \frac{v - x_{i-1}}{x_i - x_{i-1}} Q(x_k, v)\, dv. \tag{A29b}$$

Last, the discrete equations for the aerodynamical breakup contribution using the fixed-pivot technique (KR96) are given by

$$\frac{dN_i(t)}{dt} = \sum_{k=i}^{\text{NBIN}} N_k(t) P_k n_{i,k} - N_i(t) P_i. \tag{A30}$$

APPENDIX B

Generalized Exponential, Gamma, Gaussian, and Lognormal Integral Distributions

The use of a discrete method requires the integration of fragment size functions between bin limits x_i and x_{i+1} as well as functions from a similar family (order n functions), depending on the discretization scheme selected. Generalized formulations for defined integrals between bin limits x_i and x_{i+1} for some of the most common functions used in clouds microphysics (exponential, gamma, Gaussian, lognormal) as well as the definite integrals of similar functions of order n are provided

here. These generalized functions are used in the computation of terms $\kappa_{i,j,k}$ and $n_{i,k}$ in the discrete SCE–SBE. General routines to compute the value of the definite integrals over a bin size are available in the software literature (Press et al. 1992).

In the first function, the generalized gamma (exponential for $n = 0$) distribution of order n is defined by

$$\mathrm{GAM}(n) = \int_{x_1}^{x_2} x^n \exp(-ax)\, dx. \tag{B1}$$

The integration is straightforward:

$$\mathrm{GAM}(n) = -\frac{1}{a^{n+1}}[\Gamma(n+1, ax_2) - \Gamma(n+1, ax_1)], \tag{B2}$$

where $\Gamma(\alpha, x)$ is the incomplete Gamma function defined by

$$\Gamma(\alpha, x) = \int_x^{\infty} t^{\alpha-1} \exp(-t)\, dt. \tag{B3}$$

In the second function, the generalized lognormal distribution of order n is defined by

$$\mathrm{LGN}(n) = \int_{x_1}^{x_2} x^n \exp\left[-\left(\frac{\ln x - a}{b}\right)^2\right] dx, \tag{B4}$$

where $t_i = [(\ln x_i - a)/b]$. By using this change of variable, the previous integral Eq. (B4) is transformed. Consider the error function $\mathrm{erf}(x)$ defined by

$$\mathrm{erf}(x) = \frac{2}{\sqrt{\pi}} \int_0^x \exp(-t^2)\, dt. \tag{B5}$$

Then, Eq. (B4) can be integrated to give

$$\mathrm{LGN}(n) = \frac{\sqrt{\pi}}{2} b \exp\left\{(n+1)\left[a + \frac{(n+1)}{4} b^2\right]\right\}\left[\mathrm{erf}\left(t_2 - \frac{n+1}{2} b\right) - \mathrm{erf}\left(t_1 - \frac{n+1}{2} b\right)\right]. \tag{B6}$$

In the third function, the generalized Gaussian distribution of order n is defined by

$$\mathrm{GAU}(n) = \int_{x_1}^{x_2} x^n \exp\left[-\left(\frac{x-a}{b}\right)^2\right] dx. \tag{B7}$$

Taking $t_i = [(x_i - a)/b)]$, the previous integral Eq. (B7) can be rewritten into the following expression:

$$\mathrm{GAU}(n) = \int_{t_1}^{t_2} b(a+bt)^n \exp(-t^2)\, dt = \sum_{k=0}^{n} C_k^n a^{n-k} b^{k+1} \int_{t_1}^{t_2} t^k \exp(-t^2)\, dt = \sum_{k=0}^{n} C_k^n a^{n-k} b^{k+1} I_k, \tag{B8}$$

where

$$C_k^n = \frac{n!}{(n-k)!k!} \quad \text{and} \quad I_k = \int_{t_1}^{t_2} t^k \exp(-t^2)\, dt, \quad \text{with} \tag{B9}$$

$$\int_{t_1}^{t_2} t^k \exp(-t^2)\, dt = -\frac{1}{2}\int_{t_1}^{t_2} t^{k-1}\left\{\frac{d[\exp(-t^2)]}{dt}\right\} dt = -\frac{1}{2}\left[|t^{k-1}\exp(-t^2)|_{t_1}^{t_2} - \int_{t_1}^{t_2} \exp(-t^2)\left(\frac{dt^{k-1}}{dt}\right) dt\right]. \tag{B10}$$

A recursive formula is obtained and used to estimate higher-order integrals of the same family:

$$I_k = -\frac{1}{2}[|t^{k-1}\exp(-t^2)|_{t_1}^{t_2} - (k-1)I_{k-2}], \tag{B11}$$

with the initial guess depending on the value of k (odd or even). If k is even or odd, all of the integrals $I_{k\geq 2}$ or $I_{k\geq 3}$ can be estimated with the previous recursive formula starting with the initial integrals I_0 and I_1 defined by

$$I_0 = \frac{\sqrt{\pi}}{2}[\mathrm{erf}(t_2) - \mathrm{erf}(t_1)] \quad \text{and}$$

$$I_1 = -\frac{1}{2}[\exp(-t_2^2) - \exp(t_1^2)]. \tag{B12}$$

[Note: In VY85, an appendix reports similar formulas for integrating the LL82a,b parameterization between bins D_1 and D_2. However, there is a mistake in the mass-weighted integral for the case of the Gaussian dis-

tribution. When developing the formula using integration by parts, the authors appear to have used

$$C_2^3 = 2 \text{ instead of } C_2^3 = \frac{3!}{2!(3-2)!} = 3 \qquad \text{(B13)}$$

in Eq. (B10). As a result they found 1)

$$G = \frac{\sqrt{\pi}}{2}(ab^2 + a^3) \text{ instead of}$$

$$G = \frac{\sqrt{\pi}}{2}\left(\frac{3}{2}ab^2 + a^3\right) \qquad \text{(B14)}$$

and 2)

$$C_i = \frac{b^3}{2}t_i^2 + \frac{b^3}{2} + ab^2 t_i + \frac{3}{2}ba^2$$

instead of the correct expression,

$$C_i = \frac{b^3}{2}t_i^2 + \frac{b^3}{2} + \frac{3}{2}ab^2 t_i + \frac{3}{2}ba^2. \qquad \text{(B15)}$$

For convenience, notations $a = \mu$ and $b = \sqrt{2}\sigma$ have been used.]

REFERENCES

Berry, E. X., and R. J. Reinhardt, 1974: An analysis of cloud drop growth by collection: Part I. Double distributions. *J. Atmos. Sci.,* **31,** 1814–1824.

Best, A. C., 1950: Empirical formulae for the terminal velocity of water drops falling through the atmosphere. *Quart. J. Roy. Meteor. Soc.,* **76,** 302–311.

Bleck, R., 1970: A fast, approximative method for integrating the stochastic coalescence equation. *J. Geophys. Res.,* **75,** 5165–5171.

Bott, A., 1998: A flux method for the numerical solution of the stochastic collection equation. *J. Atmos. Sci.,* **55,** 2284–2293.

Brown, P. S., 1993: Analysis and parameterization of the combined coalescence, breakup, and evaporation processes. *J. Atmos. Sci.,* **50,** 2940–2951.

——, 1997: Mass conservation considerations in analytic representation of raindrop fragment distributions. *J. Atmos. Sci.,* **54,** 1675–1687.

de Beauville, C. A, R. H. Petit, G. Marion, and J. P. Lacaux, 1988: Evolution of peaks in the spectral distribution of raindrops from warm isolated maritime clouds. *J. Atmos. Sci.,* **45,** 3320–3332.

Enukashvili, I. M., 1964: On the solution of the kinetic coagulation equation. *Akad. Nauk. SSSR Izv. Geofiz. Ser.,* **10,** 944–948.

Feingold, G., S. Tzivion, and Z. Levin, 1988: Evolution of raindrop spectra. Part I: Solution to the stochastic collection/breakup equation using the method of moments. *J. Atmos. Sci.,* **45,** 3387–3399.

Gelbard, F., and J. H. Seinfeld, 1978: Numerical solution of the dynamic equation for particulate systems. *J. Comput. Phys.,* **28,** 357–375.

Hu, Z., and R. C. Srivastava, 1995: Evolution of raindrop size distribution by coalescence, breakup, and evaporation: Theory and observations. *J. Atmos. Sci.,* **52,** 1761–1783.

Khain, A. P., M. Ovtchinnikov, M. Pinsky, A. Pokrovsky, and H. Krugliak, 2000: Notes on the state-of-the-art numerical modeling of cloud microphysics. *Atmos. Res.,* **55,** 159–224.

Komabayasi, M., T. Gonda, and K. Isono, 1964: Lifetime of water drops before breaking and size distribution of fragment droplets. *J. Meteor. Soc. Japan,* **42,** 330–340.

Kovetz, A., and B. Olund, 1969: The effect of coalescence and condensation on rain formation in a cloud of finite vertical extent. *J. Atmos. Sci.,* **26,** 1060–1065.

Kumar, S., and D. Ramkrishna, 1996: On the solution of population balance equations by discretization—I. A fixed pivot technique. *Chem. Eng. Sci.,* **51,** 1311–1332.

Lang, J. L., and A. P. Barros, 2002: An investigation of the onsets of the 1999 and 2000 monsoons in central Nepal. *Mon. Wea. Rev.,* **130,** 1299–1316.

List, R., and J. R. Gillespie, 1976: Evolution of raindrop spectra with collision-induced breakup. *J. Atmos. Sci.,* **33,** 2007–2013.

——, and G. M. McFarquhar, 1990: The role of breakup and coalescence in the three-peak equilibrium distribution of raindrops. *J. Atmos. Sci.,* **47,** 2274–2292.

——, N. R. Donaldson, and R. E. Stewart, 1987: Temporal evolution of drop spectra to collisional equilibrium in steady and pulsating rain. *J. Atmos. Sci.,* **44,** 362–372.

Long, A. B., 1974: Solutions to the droplet collection equation for polynomial kernels. *J. Atmos. Sci.,* **31,** 1040–1052.

Low, T. B., and R. List, 1982a: Collision, coalescence and breakup of raindrops. Part I: Experimentally established coalescence efficiencies and fragment size distributions in breakup. *J. Atmos. Sci.,* **39,** 1591–1606.

——, and ——, 1982b: Collision, coalescence and breakup of raindrops. Part II: Parameterization of fragment size distributions. *J. Atmos. Sci.,* **39,** 1607–1618.

Mahoney, A. W., and D. Ramkrishna, 2002: Efficient solution of population balance equations with discontinuities by finite elements. *Chem. Eng. Sci.,* **57,** 1107–1119.

Marshall, J. S., and W. McK. Palmer, 1948: The distribution of raindrops with size. *J. Atmos. Sci.,* **5,** 165–166.

McFarquhar, G. M., 2004: A new representation of collision-induced breakup of raindrops and its implications for the shapes of raindrop size distributions. *J. Atmos. Sci.,* **61,** 777–794.

——, and R. List, 1993: The effect of curve fits for the disdrometer calibration on raindrop spectra, rainfall rate, and radar reflectivity. *J. Appl. Meteor.,* **32,** 774–782.

McTaggart-Cowan, J. D., and R. List, 1975: Collision and breakup of water drops at terminal velocity. *J. Atmos. Sci.,* **32,** 1401–1411.

Prat, O. P., and A. P. Barros, 2007: Exploring the use of a column model for the characterization of microphysical processes in warm rain: Results from a homogeneous rainshaft model. *Adv. Geosci.,* **10,** 145–152.

Press, W. H., S. A. Teukolsky, W. T. Vetterling, and B. P. Flannery, 1992: *Numerical Recipes in Fortran; The Art of Scientific Computing*. 2d ed. Cambridge University Press, 915 pp.

Pruppacher, H. R., and J. D. Klett, 1978: *Microphysics of Clouds and Precipitation.* D. Reidel, 714 pp.

Seifert, A., A. Khain, U. Blahak, and K. D. Beheng, 2005: Possible effects of collisional breakup on mixed-phase deep convection simulated by a spectral (bin) cloud model. *J. Atmos. Sci.,* **62,** 1917–1931.

Sheppard, B. E., 1990: Effect of irregularities in the diameter clas-

sification of raindrops by the Joss–Waldvogel disdrometer. *J. Atmos. Oceanic Technol.,* **7,** 180–183.

Srivastava, R. C., 1971: Size distribution of raindrops generated by their breakup and coalescence. *J. Atmos. Sci.,* **28,** 410–415.

Testik, F. Y., and A. P. Barros, 2007: Toward elucidating the microstructure of rainfall: A survey. *Rev. Geophys.,* **45,** RG2003, doi:10.1029/2005RG000182.

Tzivion, S., G. Feingold, and Z. Levin, 1987: An efficient numerical solution to the stochastic collection equation. *J. Atmos. Sci.,* **44,** 3139–3149.

Valdez, M. P., and K. C. Young, 1985: Number fluxes in equilibrium raindrop populations: A Markov chain analysis. *J. Atmos. Sci.,* **42,** 1024–1036.

Zawadzky, I., and M. de Agostinho Antonio, 1988: Equilibrium raindrop size distributions in tropical rain. *J. Atmos. Sci.,* **45,** 3452–3459.

CORRIGENDUM

Because of a production error in "A Robust Numerical Solution of the Stochastic Collection–Breakup Equation for Warm Rain," by Olivier P. Prat and Ana P. Barros, which appeared in the *Journal of Applied Meteorology and Climatology,* Vol. 46, No. 9, 1480–1497, the incorrect variable E_{coal} (coalescence efficiency) appeared in print in three places on p. 1482 instead of the correct variable E_{coll} (collision efficiency). The corrected Eq. (3) should read as

$$K(v, v') = (9\pi/16)^{1/3}(v^{1/3} + v'^{1/3})^2|\mathbf{V} - \mathbf{V}'|E_{\text{coll}}(v, v'). \quad (3)$$

In addition, the remainder of the paragraph that appears further down immediately below Eq. (4) should read ". . . where **V** is in centimeters per second and d, the diameter of the drop, is in centimeters; $E_{\text{coll}}(v, v')$ is the collision efficiency. For the drop sizes considered in this study ($d \geq 0.01$ cm), $E_{\text{coll}}(v, v') = 1$, as per Long (1974)."

The staff of the *Journal of Applied Meteorology and Climatology* regrets any inconvenience this error may have caused.